MULTI-ALGORITHM CLASSIFICATION AND CA‐MARKOV PREDICTION OF LAND-USE CHANGE ACROSS THREE TEMPORAL INTERVALS: A CASE STUDY OF THE LOE TOR ROYAL PROJECT, TAK PROVINCE, THAILAND

Sorawit ONPHUA [1], Sakhan TEEJUNTUK [1,2*] & Chakrit NA TAKUATHUNG [1]

DOI: 10.21163/GT_2026.212.11

ABSTRACT

Land-use and land-cover (LULC) change in mountainous watersheds has significant implications for food security, biodiversity conservation, and carbon storage. This study assessed LULC dynamics in the Loe Tor Royal Project area, Tak Province, Thailand, using multi-temporal satellite imagery (2006‐2026), five supervised classification algorithms (Random Forest, Artificial Neural Network, Linear Discriminant Analysis, Support Vector Machine, and XGBoost), and CA‐Markov spatial modeling across three calibration intervals (3-year, 5-year, and 10-year). Between 2006 and 2026, forest cover declined from 64.10% to 45.16%, while agricultural land expanded from 8.29% to 30.82%, with the rate of agricultural expansion accelerating markedly in recent years. Cramér's V analysis identified distance to settlements (V = 0.85), distance to roads (V = 0.67), and elevation (V = 0.61) as the most influential spatial drivers of LULC transitions. Among the three calibration intervals, the 3-year model achieved the highest validation accuracy, whereas the 10-year model performed substantially worse, indicating that shorter calibration intervals produce more reliable CA‐Markov projections. The inferior performance of the 10-year model is attributed to Markov non-stationarity over extended calibration periods and cross-sensor spectral inconsistencies, highlighting the important methodological consideration for CA-Markov applications using multi-sensor datasets. Under Business-as-usual scenarios, forest cover is projected to continue declining, with agricultural land expanding progressively along low elevation zones near road networks and settlements, reaching approximately 42.7% by 2035 under the 3-year scenario. These findings highlight the ecological vulnerability of this critical watershed and emphasize the need for protective buffer zones, conservation agriculture practices, and degraded land rehabilitation efforts.

Keywords: *LULC change; CA–Markov model; Multi-algorithm classification; Calibration interval comparison; Sentinel-2; Landsat; Watershed management.*

1. INTRODUCTION

Land-use and land-cover (LULC) change is one of the most direct indicators of human–environment interaction, and in mountainous watersheds it carries significant implications for food security, biodiversity conservation, carbon storage, and hydrological regulation(Wang et al., 2023). The Loe Tor Royal Project, located in Mae Ramat District, Tak Province, is a site of considerable importance for natural resource restoration and soil and water management (Royal Development Projects Board, 2025). As a critical watershed draining into both the Salween and Ping river systems, the area provides ecosystem services on which downstream communities and agriculture depend; unplanned agricultural expansion into forested land can therefore trigger ecosystem degradation, accelerated soil erosion, and long-term environmental decline (Wang et al., 2023). Reliable, spatially explicit information on the rate, direction, and likely future trajectory of LULC change is thus essential — for local communities whose livelihoods depend on these resources, and for the

[1] *Faculty of Forestry, Kasetsart University, Bangkok 10900, Thailand ;*
sorawit.on@ku.th (SO), fforsktt@ku.ac.th (ST), chakrit.n@ku.ac.th (CN).
[2] *Princess Sirindhorn Center for Sustainable Development, Kasetsart University, Bangkok 10900, Thailand.*
[*] *Corresponding author : fforsktt@ku.ac.th (ST).*

government and Royal Project agencies responsible for land-use zoning and watershed protection. Geographic information systems and remote sensing provide the means to generate such information and to identify priority areas for intervention (Butt et al., 2015).

The trajectory of LULC change is governed by both biophysical and anthropogenic driving variables whose relative influence varies across geographic settings. Biophysical factors such as elevation and slope constrain the suitability of land for cultivation, whereas accessibility-related factors — particularly proximity to roads and settlements — shape the intensity and location of human activity (Thammanu et al., 2020). Recent geo-informatic studies in Thailand have quantified how these drivers translate into measurable transitions: Kiriwongwattana and Waiyasusri (2024) traced tourism-driven expansion of built-up land in Phuket, while Waiyasusri (2021) characterised mangrove and urbanisation dynamics in the Krabi Estuary Wetland using spectral indices. Identifying the dominant drivers in a given landscape is therefore a prerequisite for credible modelling and projection of future change.

A range of models has been developed to project future LULC, each differing in data requirements and spatial behaviour. The Markov chain estimates the quantity and probability of transitions between classes from historical change but is spatially non-explicit (Nouri et al., 2014). Cellular automata (CA) introduce spatial allocation through neighbourhood interactions and transition rules (Mansour et al., 2020). The integrated CA–Markov model couples the temporal prediction of the Markov chain with the spatial allocation of CA, producing spatially explicit projections from comparatively few inputs; it has been widely applied for forest-change projection in tropical settings, for example by Sari et al. (2025), in this journal, who coupled Land Change Modeler with CA–Markov to project forest-to-non-forest conversion in Boven Digoel, Indonesia, using driver variables comparable to those employed here. By contrast, the CLUE-s and Dyna-CLUE models allocate change through empirical relationships between land use and multiple socio-economic and biophysical drivers and are well suited to multi-scenario policy analysis — for example, Waiyasusri and Chotpantarat (2022) applied the Dyna-CLUE model to project coastal land-use change in Koh Chang — but they require extensive driver datasets that are often unavailable for remote highland watersheds. Given the data constraints of the Loe Tor area and the spatially explicit objective of this study, the CA–Markov model offers the most appropriate balance of robustness, reproducibility, and data efficiency.

To extract spatially explicit land-use information, multi-temporal satellite imagery was classified into thematic categories (MohanRajan et al., 2020). Because no single algorithm performs optimally across all sensors and landscapes, five supervised classifiers — Random Forest (RF), Artificial Neural Network (ANN), Linear Discriminant Analysis (LDA), Support Vector Machine (SVM), and XGBoost (XGB) — were compared to identify the best-performing classifier for each study year, an approach also adopted in recent multi-algorithm classification studies in Thailand (Worachairungreung et al., 2023). Statistical differences among classifiers were assessed using Cochran's Q and McNemar tests (Cochran, 1950), and classification accuracy was evaluated using Overall Accuracy, Producer's and User's Accuracy, and the Kappa coefficient (Congalton, 2001). The association between categorical spatial drivers and observed LULC transitions was quantified using Cramér's V (Akoglu, 2018).

Despite extensive LULC research in Thailand, three gaps remain. First, many studies rely on a single classifier, leaving the comparative behaviour of multiple machine-learning algorithms in spectrally heterogeneous highland terrain under-examined. Second, the sensitivity of CA–Markov projections to the length of the calibration interval is rarely tested, even though the choice of interval directly affects the stationarity assumption underlying the Markov process. Third, royal-initiative highland watersheds such as Loe Tor remain under-studied despite their conservation significance and their reliance on multi-sensor imagery spanning two decades. The present study addresses these gaps by comparing five classifiers and, in particular, by systematically evaluating three CA–Markov calibration intervals (3-, 5-, and 10-year) against a common 2026 validation reference — a methodological comparison that, to our knowledge, has not previously been reported for a multi-sensor highland LULC dataset.

Accordingly, this study aims to: (1) classify multi-temporal LULC (2006–2026) using five machine-learning algorithms and multi-source satellite imagery (Landsat 5, Landsat 8, and Sentinel-2); (2) identify the key spatial drivers of LULC transitions using Cramér's V analysis; (3) compare the predictive performance of three CA–Markov calibration intervals (3-year, 5-year, and 10-year); and (4) project future LULC scenarios under Business-as-Usual conditions to support watershed-management strategies. The expected outputs are a set of accuracy-assessed LULC maps, inter-class transition matrices, a calibration-interval performance comparison, and validated near-future projections that together provide an evidence base for land-use planning at Loe Tor and methodological guidance for CA–Markov applications in multi-sensor mountainous settings.

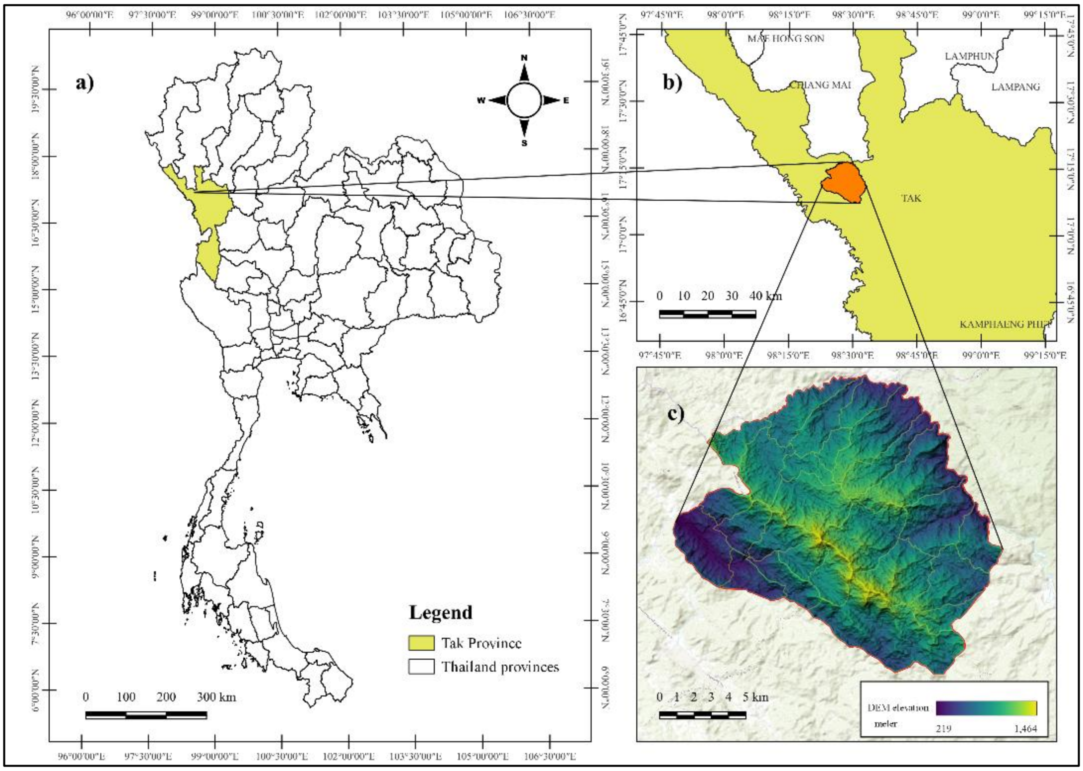

Fig. 1. Location of the Loe Tor Royal Project study area, Mae Ramat District, Tak Province, Thailand. (a) Tak Province within Thailand; (b) study-area boundary between the Salween (west) and Ping (east) watersheds; (c) digital elevation model (219–1,464 m a.s.l.).

2. STUDY AREA

The research was conducted at the Loe Tor Royal Project area located in Mae Ramat District, Tak Province. The area covers approximately 20,250 hectares (ha) (**Fig. 1**) and encompasses 26 villages (Royal Development Projects Board, 2025). This site constitutes a critical watershed draining westward into the Salween River and eastward into the Ping River, which flows into the Chao Phraya River. The landscape is characterized by complex mountainous terrain, with elevations ranging from 219 to 1,464 meters above sea level (Royal Project Foundation, 2025). Forest vegetation is highly diverse, including mixed deciduous forest, deciduous dipterocarp, and hill evergreen forest types (Thammanu et al., 2020). The regional climate is defined by three distinct seasons: rainy (June–October), winter (November–February), and summer (March–May).

3. DATA AND METHODS

3.1. Data Types and Sources

This study integrates four satellite data sources to enable temporal analysis across three periods (**Table 1**). Landsat 5 imagery (2006, 30 m) was used to provide the historical baseline for the 10-year interval analysis. Landsat 8 imagery (2016, 30 m) represents the intermediate period. Sentinel-2 imagery (2020, 2021, 2023, 2026; 10 m) supports both 3-year and 5-year interval analyses. All images were acquired during the dry season (February) to minimize cloud contamination and reduce phenological variability.

Table 1.

Data Types and Sources of sensor

Sensor	Year	Path/Row	Acquisition	Bands Used	Resolution	Analysis Period
Landsat 5 TM	2006	131/048	Feb 2006	1–5, 7	30 m	10-year
Landsat 8 OLI	2016	131/048	Feb 2016	2–7	30 m	10-year / 5-year
Sentinel-2 L2A	2020	47N	Feb 2020	2–8A, 11–12	10 m	3-year
Sentinel-2 L2A	2021	47N	Feb 2021	2–8A, 11–12	10 m	5-year
Sentinel-2 L2A	2023	47N	Feb 2023	2–8A, 11–12	10 m	3-year
Sentinel-2 L2A	2026	47N	Feb 2026	2–8A, 11–12	10 m	3-year / 5-year / 10-year (ref)

To ensure cross-sensor spatial consistency, Sentinel-2 imagery (10 m) was resampled to 30 m using bilinear interpolation when combined with Landsat data for the 5-year and 10-year interval analyses, whereas the 3-year analysis retained native 10 m resolution. Land-use change detection was conducted using the Post Classification Comparison (PCC) approach, which involves independent classification of each image followed by map comparison, thereby reducing the influence of sensor-specific spectral differences. (Sharma and Sharma, 2024). However, it should be noted that PCC does not fully account for differences in Spectral Response Functions (SRFs) among sensors (Claverie et al., 2018). This limitation is further discussed in Section 4.

3.2. Land-Use Classification

Land-use and Land cover (LULC) was classified into five thematic categories as Forest, Agriculture, Urban/Village, Grassland, and Degraded Forest **(Table 2)**. LULC classification was conducted using five supervised algorithms implemented in R as (1) Random Forest (RF; ranger package, ntree = 500, tuneLength = 5); (2) Artificial Neural Network (ANN; nnet package via caret, tuneLength = 5); (3) Linear Discriminant Analysis (LDA; MASS package via caret); (4) Support Vector Machine (SVM; e1071 package via caret, radial basis function kernel, tuneLength = 5); and (5) XGBoost (XGB; xgboost package, max depth = 6, learning rate $\eta = 0.1$, subsample = 0.8, col sample by tree = 0.8, with 5-fold cross-validation and early stopping at 20 rounds). All caret models (RF, ANN, LDA, SVM) were trained using 5-fold cross-validation. The dataset was partitioned into 70% training and 30% testing subsets using stratified random partitioning (caret: createDataPartition). All classifier were trained using the same 12 predictor variables, comprising five spectral bands (Blue, Green, Red, NIR, and SWIR calculated as the mean of Sentinel-2 B11 and B12 or Landsat SWIR1 and SWIR2), four spectral indices (NDVI, NDBI, MNDWI, EVI), and three topographic variables (DEM, Slope, Aspect). For Sentinel-2 imagery, SWIR bands B11 and B12 (20 m native resolution) were resampled to 10 m using bilinear interpolation prior to computing the composite SWIR band. For each study year, the best-performing classification was selected based on Overall Accuracy (OA).Statistical differences among classifiers were tested using Cochran's Q test (Cochran (1950); $\alpha = 0.01$), followed by pairwise post-hoc comparisons using McNemar tests (Bonferroni-corrected). Training samples were collected using stratified random sampling with a minimum of 100 reference points per land-use category per year.

Table 2.
Descriptions of Land Use and Land Cover (LULC) categories

LULC Category	Description
Forest	Areas dominated by tree cover, perennial vegetation, and economic forest plantation, including specific forest types such as dry evergreen, mixed deciduous forest, deciduous dipterocarp, and hill evergreen forest type.
Agriculture	Areas used for agricultural production including cultivated cropland (e.g., maize, cassava), irrigated land, and scattered village settlements.
Urban/Village	Areas comprising village settlements, residential structures and infrastructures including offices of forestry units and other government departments.
Grassland	Areas covered by grass and ferns, with the absence of large trees or saplings.
Degraded Forest	Open or prepared land with fewer than approximately 13 trees per hectare

3.3. Accuracy Assessment

Classification accuracy was evaluated by comparing the classified maps with independent validation samples obtained from high-resolution imagery and field observations. Four standard metrics were computed: Overall Accuracy (OA), Producer's Accuracy (PA), User's Accuracy (UA), and the Kappa coefficient (Cohen, 1960) Overall Accuracy and the Kappa coefficient were calculated as shown in Eqs. **(1)** and **(2)**, respectively. The strength of classification agreement was interpreted according the thresholds proposed by Congalton (2001).

$$OA = \left(\frac{\sum Xii}{N}\right) * 100 \tag{1}$$

$$K = \frac{N\sum_{i=1}^{r} Xii - \sum_{i=1}^{r}(Xi+)*(X+i)}{N^2 - \sum_{i=1}^{r}(Xi+)*(X+i)} \tag{2}$$

where:

K	-Kappa coefficient
R	-Number of rows in the matrix
$X_{(ii)}$	-Number of observations in row i and column i (diagonal elements)
$X_{(i+)}$	-Total number of observations in row I
$X_{(+i)}$	-Total number of observations in column I
N	-Total number of observations or verification points

3.4. Driver Variable Analysis

Seven spatial driver variables influencing LULC change were evaluated: elevation (DEM), slope, aspect, hillshade, distance to roads (dist_road), distance to streams (dist_stream), and distance to villages or settlements (dist_settle). The relative importance of these variables was assessed using Cramér's V statistic (Akoglu, 2018) for each transition pair, providing a quantitative measure of association between individual spatial drivers and the observed LULC transitions.

These seven variables were selected on three criteria: (i) their established relevance as biophysical or accessibility drivers of LULC change in mountainous watersheds (Pande et al., 2018), (ii) the availability of reliable, spatially complete layers for the entire study area across all time points; and (iii) low redundancy, which was subsequently confirmed through the pairwise Cramér's V matrix **(Table 7).**

3.5. CA–Markov Model and Multi-Temporal Analysis

Spatial modelling and LULC change prediction were conducted using R with the terra and ranger packages, implementing a CA–Markov modeling framework. For each of the three temporal intervals, a Markov transition probability matrix was derived from the transition between T1 and T2. Spatial transition suitability maps were generated using 20 Random Forest (RF) binary classification models, corresponding to each possible transition pair. The CA neighborhood module applied a 5×5 Moore window to account for spatial contiguity in land-use transitions. A total of 40,000 spatially random sample points were extracted from the T1 and T2 LULC maps together with the seven driver variables to train the RF transition models. Each binary RF classifier was trained using balanced sampling, with a maximum of 8,000 samples per class and 500 trees. The CA neighborhood influence weight was set to 0.5, meaning that the transition suitability score for each pixel was adjusted by 50% of the proportion of neighboring pixels already belonging to the target land-use class.

The CA–Markov framework couples Markov-chain temporal prediction with cellular-automata spatial allocation. The Markov component estimates the system state at the next time step from the current state and a transition probability matrix:

$$S(t+1) = Pij * S(t) \quad (3)$$

where P_{ij} is the transition probability matrix derived from two reference dates ($0 \leq P_{ij} < 1$; $\Sigma_j P_{ij} = 1$). Because the Markov chain is spatially non-explicit, the cellular-automata component allocates the predicted change in space:

$$S(x, t+1) = f(S(x,t), \Omega(x)) \quad (4)$$

where $\Omega(x)$ is the neighbourhood of cell x (a 5×5 Moore window) and f combines the Markov-derived transition area, the Random-Forest-based transition suitability, and the neighbourhood weight (0.5).

Three independent CA–Markov models were calibrated and validated as followed:

- 3-year interval: calibrated in 2020 to 2023, validated against 2026
- 5-year interval: calibrated in 2016 to 2021, validated against 2026
- 10-year interval: calibrated in 2006 to 2016, validated against 2026

The year 2026 (Sentinel-2 imagery) serves as the common independent validation reference across all three models. Future LULC projections were generated at one-interval steps beyond 2026: the 3-year model projects to 2029, 2032, and 2035; the 5-year model to 2031, 2036, and 2041; and the 10-year model to 2036, 2046, and 2056.

3.6. Model Validation

Model performance was evaluated using four complementary metrics following Pontius et al. (2007) and Pontius and Millones (2011).

These metrics included;

- Overall Accuracy (OA): the proportion of correctly predicted pixels across all land-use classes.
- Kappa Coefficient (K): the adjustment of OA for chance agreement (Cohen, 1960).
- Figure of Merit (FOM): the measurement of agreement exclusively for pixels that experienced change (FOM = A/[A+B+C]) with benchmark values typically range from 0.05–0.30 (Pontius et al., 2007)
- Quantity Disagreement (QD) and Allocation Disagreement (AD): the decompose of total classification error into error related to class proportion mismatch and spatial misallocation (Pontius et al., 2007).

Model validation was conducted using 2,500 stratified random sample points (500 per LULC class), extracted independently from the observed 2026 Sentinel-2 classification map. This stratified design ensures balanced representation of all land-use classes, including those occupying small proportions of the study area (Olofsson et al., 2014).

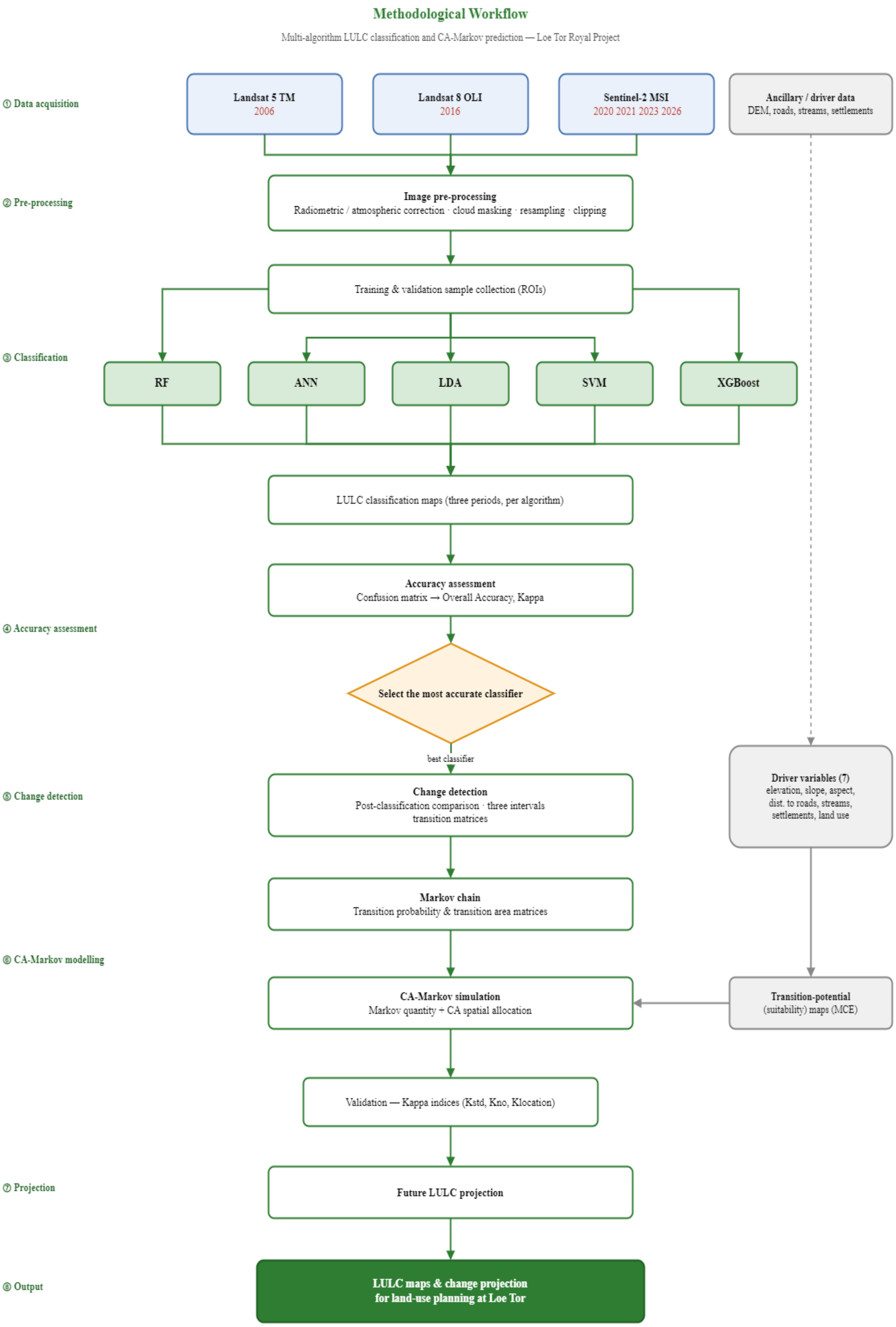

Fig. 2. Methodological workflow of the study.

4. RESULTS AND DISCUSSIONS

4.1. LULC Classification Accuracy

Six multi-temporal satellite images (2006–2026) were classified using five machine learning algorithms. Overall, classification performance is summarized in **Table 3**. Sentinel-2 imagery (10 m) consistently achieved higher accuracy (OA = 83.4–90.9%) than Landsat data (OA = 78.1–86.1%), a difference attributable to Sentinel-2's spatial resolution and enhanced spectral capabilities. Kappa coefficients ranged from 0.70 (Substantial agreement) to 0.88 (Almost Perfect agreement), indicating reliable classification performance across all years. Cochran's Q test revealed statistically significant differences among the five models in every year ($p < 0.01$), with SVM consistently exhibiting the lowest performance. Classified LULC maps for all six study years, along with classifier comparison insets, are presented in **(Fig. 3).**

Table 3.

Summary of classification accuracy across all study years.

Year	Sensor	Best Model	OA (%)	Kappa	F1 (%)	Agreement	Cochran Q	Interval
2006	Landsat 5	RF	78.1	0.7047	73.3	Substantial	18.41***	**10-yr (T1)**
2016	Landsat 8	ANN	86.1	0.8133	82.3	Almost Perfect	16.40**	**10-yr (T2) / 5-yr (T1)**
2020	Sentinel-2	LDA	90.9	0.8793	89.1	Almost Perfect	50.82***	**3-yr (T1)**
2021	Sentinel-2	RF	85.6	0.8068	82.3	Substantial	60.39***	**5-yr (T2)**
2023	Sentinel-2	RF	83.4	0.7793	79.7	Substantial	26.55***	**3-yr (T2)**
2026	Sentinel-2	LDA	88.8	0.8496	86.8	Almost Perfect	61.21***	**Validation**

**** $p < 0.001$; ** $p < 0.01$. Agreement categories follow Congalton (2001).*

The higher classification accuracy obtained from Sentinel-2 imagery (OA = 83.4–90.9%) compared to Landsat data (OA = 78.1–86.1%) is consistent with finding from recent comparative studies. Madiela et al. (2024) reported that Sentinel-2 (OA = 93.8%) outperformed Landsat 9 (OA = 91.6%) in LULC classification within the Congo Basin rainforest, attributing the improvement to Sentinel-2's finer spatial resolution (10 m vs. 30 m) and additional red-edge bands that enhance vegetation discrimination. Similarly, Keyamf et al. (2023) found that Sentinel-2 achieved an accuracy of 91%, compared to 85% for Landsat-8, when mapping shifting agricultural landscapes in Cameroon, particularly in the delineation of small-size LULC units.

The finding that no single classification algorithm consistently outperformed other across all years where RF performing best in 2006, 2021, and 2023, while LDA excelled in 2020 and 2026, highlights the sensitivity of classifier performance to data characteristics and class separability. This result is aligned with Aftab et al. (2024), who demonstrated that optimal algorithm performance varies with landscape complexity, sensor type, and the spectral characteristics of target classes. The consistently lower performance of SVM further corroborates findings by Basheer et al. (2022), who reported that ensemble-based methods, such as RF, XGBoost, generally outperform kernel-based classifiers in heterogeneous tropical environments.

Table 4 summarizes the five most important predictor variables for the Random Forest classifier across all study years. Spectral bands (Red, Blue, Green, and SWIR) and vegetation indices (NDVI and NDBI) consistently ranked highest, whereas topographic variables (DEM, Slope, and Aspect) contributed relatively less to overall classification accuracy. The observed transition from optical-band dominance (Green and Red) during the Landsat era (2006–2016) to index-based dominance (NDVI, NDBI, SWIR) in the Sentinel-2 imagery (2020–2026) reflects the enhanced spectral information, available from the newer sensor platform.

Table 4.

Top five predictor variables by relative importance (%) for each study year.

Rank	2006	2016	2020	2021	2023	2026
1	Green (100.0)	Blue (100.0)	Red (99.7)	SWIR (100.0)	NDVI (100.0)	NDVI (99.5)
2	Red (96.2)	Green (72.2)	NDVI (99.6)	NDVI (89.1)	SWIR (87.9)	Red (98.9)
3	SWIR (74.9)	MNDWI (53.2)	Blue (99.4)	NDBI (83.2)	NDBI (75.7)	NDBI (98.5)
4	Blue (45.9)	DEM (35.7)	SWIR (99.4)	Green (42.9)	Red (53.4)	SWIR (97.7)
5	NIR (41.6)	EVI (31.9)	Green (98.3)	Blue (41.2)	Blue (47.8)	Blue (96.0)

Values in parentheses represent relative importance (%). Importance normalized to 0–100 scale within each year.

Table 5.

Per-class CA–Markov prediction accuracy by temporal interval (validated against 2026).

Class	3-Year			5-Year			10-Year		
	PA	UA	F1	PA	UA	F1	PA	UA	F1
Forest	0.8159	0.7653	0.7898	0.8295	0.6695	0.7410	0.6757	0.5246	0.5906
Agriculture	0.7166	0.7077	0.7121	0.5784	0.7283	0.6448	0.1497	0.5355	0.2340
Urban/Village	0.3772	0.1458	0.2103	0.2348	0.1149	0.1543	0.2344	0.0763	0.1152
Grassland	0.3632	0.6638	0.4695	0.2233	0.7385	0.3429	0.2783	0.1777	0.2169
Degraded Forest	0.1762	0.5000	0.2606	0.2834	0.4070	0.3341	0.0524	0.1429	0.0767
OA / Kappa	**0.6592 / 0.4922**			**0.6160 / 0.4134**			**0.3940 / 0.1141**		

PA = Producer's Accuracy; UA = User's Accuracy; F1 = harmonic mean of PA and UA.

The 3-year interval model achieved the highest overall accuracy (OA = 0.6592, Kappa = 0.4922), followed by the 5-year model (OA = 0.6160, Kappa = 0.4134) and 10-year model (OA = 0.3940, Kappa = 0.1141). Across all intervals, the forest class consistently exhibited the highest F1 scores. In contrast, the Urban/Village and Degraded Forest classes demonstrated lower accuracy, primarily due to spectral confusion. Per-class prediction accuracy across all intervals is detailed in **(Table 5).**

Table 6.

LULC area comparison across three temporal intervals.

3-year Interval (2020, 2023, 2026)						
LULC Class	**2020 (ha)**	**2020 (%)**	**2026 (ha)**	**2026 (%)**	**Net Δ (ha)**	**Δ/yr (ha)**
Forest	9867.4	48.95	9104.1	45.16	-763.2	-127.2
Agriculture	3102.8	15.39	6213.0	30.82	+3110.2	+518.4
Urban/Village	1869.8	9.28	990.4	4.91	-879.4	-146.6
Grassland	2846.1	14.12	1750.7	8.68	-1095.4	-182.6
Degraded Forest	2471.6	12.26	2099.5	10.42	-372.2	-62.0
5-year Interval (2016, 2021, 2026)						
LULC Class	**2016 (ha)**	**2016 (%)**	**2026 (ha)**	**2026 (%)**	**Net Δ (ha)**	**Δ/yr (ha)**
Forest	10943.6	54.29	9104.1	45.16	-1839.5	-183.9
Agriculture	2095.6	10.40	6213.0	30.82	+4117.4	+411.7
Urban/Village	2215.1	10.99	990.4	4.91	-1224.7	-122.5
Grassland	2745.0	13.62	1750.7	8.68	-994.3	-99.4
Degraded Forest	2158.4	10.71	2099.5	10.42	-58.9	-5.9
10-year Interval (2006, 2016, 2026)						
LULC Class	**2006 (ha)**	**2006 (%)**	**2026 (ha)**	**2026 (%)**	**Net Δ (ha)**	**Δ/yr (ha)**
Forest	12921.8	64.10	9104.1	45.16	-3817.6	-190.9
Agriculture	1671.0	8.29	6213.0	30.82	+4542.0	+227.1
Urban/Village	2011.4	9.98	990.4	4.91	-1021.1	-51.1
Grassland	1410.6	7.00	1750.7	8.68	+340.1	+17.0
Degraded Forest	2142.8	10.63	2099.5	10.42	-43.4	-2.2

Δ = change from first to last year of each interval. Negative values indicate area loss.

Across the 20-year observation period (2006–2026), the net forest loss reached 3,817.6 ha, corresponding to an average annual loss of approximately 190.9 ha. The majority of this lost forest area was converted to agriculture land, which expanded by 4,542.0 ha over the same period. Notably, the rate of agricultural expansion increased substantially in recent years, raising from 227.1 ha/year during the 10-year interval to 518.4 ha/year over the most recent 3-year interval (2020–2026). This continuous and accelerating transition highlights intensifying economic and agricultural pressure on forest, with significant implications for LULC changes, local climate and biodiversity (**Fig. 3**).

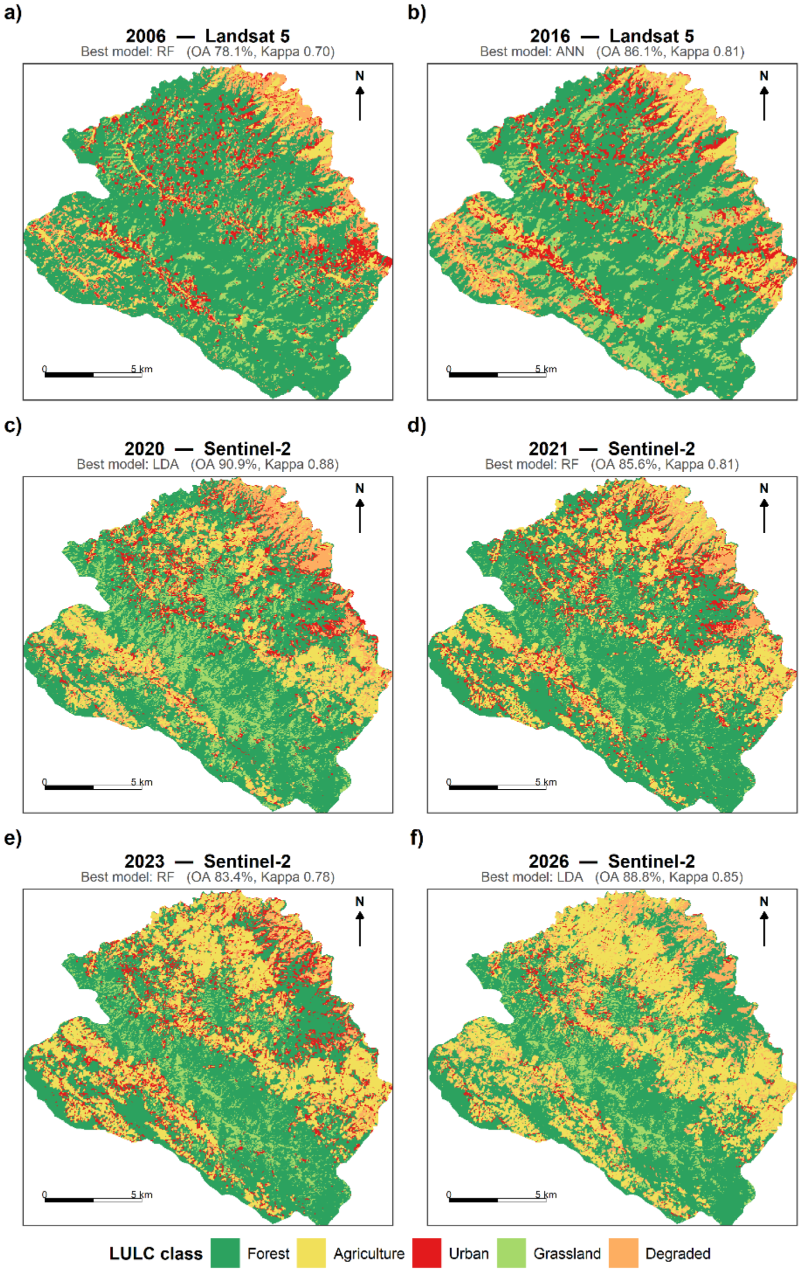

Fig. 3. Classified LULC maps for the six study years (a–f: 2006, 2016, 2020, 2021, 2023, 2026), each produced by the best-performing classifier, with five-classifier comparison insets (red box). Classes: Forest, Agriculture, Urban/Village, Grassland, Degraded Forest.

4.2. LULC Change Analysis

The analysis of land use changes in the Loe Tor Royal Project area across multiple temporal intervals (2006–2016, 2016–2021, and 2020–2023–2026) revealed that the most significant transformations occurred within the Forest and Agriculture categories. Across all intervals, forest cover exhibited consistent decline, while agricultural land expanded, reflecting a clear pattern of forest conversion to agricultural use. The 10-year interval (2006–2026) captured the largest absolute magnitude of change, with forest area decreasing by 3,817.6 ha and agricultural land increasing by 4,542.0 ha. In contrast, the 3-year interval showed the marked recent acceleration in agricultural expansion, increasing of 3,110.2 ha over the 6 years period. These findings are consistent with Bairwa et al. (2025), who identified the conversion of forested land to agriculture as a primary global driver of deforestation.

Table 6 presents area statistics for each LULC class across all study years. Across all three temporal intervals, forest cover exhibited a consistent declining trend, whereas agricultural land demonstrated continuous expansion. In the 3-year interval (2020–2026), forest area decreased from 9,867.4 ha (48.95%) to 9,104.1 ha (45.16%), representing a net loss of 763.2 ha (–127.2 ha/yr). In contrast, agricultural land increased from 3,102.8 ha (15.39%) to 6,213.0 ha (30.82%), corresponding to a net gain of 3,110.2 ha (+518.4 ha/yr), thereby confirming direct forest conversion to agricultural use over this period. Similar patterns were observed during the 5-year interval (2016–2026), in which agricultural land expanded by 4,117.4 ha (+411.7 ha/yr), primarily at the expense of forest (–1,839.5 ha) and Urban/Village areas (–1,224.7 ha). The 10-year interval (2006–2026) captured the largest absolute magnitude of change, with agriculture land increasing by 4,542.0 ha (+227.1 ha/yr) and forest cover declining by 3,817.6 ha (–190.9 ha/yr). Across all intervals, the progressive acceleration of agricultural expansion from 227.1 ha/yr in the 10-year interval to 518.4 ha/yr in the 3-year intervals, underscores the intensifying pressure on remaining forest cover in recent years.

The accelerating rate of forest-to-agriculture conversion identified in this study (from 190.9 ha/yr over 20 years to 518.4 ha/yr in the most recent 6-year period) mirrors regional deforestation trends observed across mainland Southeast Asia. Zhai et al. (2023) reported that the region experienced some of the highest deforestation rates globally, driven predominately by agricultural expansion into highland forest areas, a pattern consistent with the dynamics observed in the Loe Tor Royal Project area. The expansion of maize and cassava cultivation as a principle drivers of upland deforestation in northern Thailand has been documented by Hurni and Fox (2018). The result identified market integration and increasing road accessibility as key catalysts of this process findings that align closely with Cramér's V study, in which distance to settlements (V = 0.85) and distance to roads (V = 0.67) emerged as the most influential drivers.

The observed decline in Urban/Village area from 9.98% in 2006 to 4.91% in 2026 appears counterintuitive and is unlikely reflects an actual reduction in settlement extent. As noted by Bai et al. (2025), spectral confusion between bare agricultural soil and built-up surfaces in mountainous landscape frequently leads to overestimation of urban or village areas in Landsat-based classifications, a bias that tends to be corrected when higher-resolution Sentinel-2 imagery becomes available. This sensor-dependent reclassification effect should therefore be carefully considered when interpreting long-term LULC trends across multi-sensor datasets.

4.3. Driver Variable Analysis and Multicollinearity

Cramér's V analysis indicated that accessibility-related variables are the dominant drivers of LULC transitions. Among the examined factors, distance to settlements exhibited the highest V value (0.8452), suggested that areas located closer to villages are highly susceptible to land transformation. Distance to roads emerged as the second most influential factor (V = 0.6691), underscoring the importance of transportation infrastructure in facilitating agricultural expansion and forest conversion. Elevation (DEM) also demonstrated a strong association (V = 0.6060), particularly in governing transitions between forest and grassland in higher altitude zones. In contrast, variables slope, stream proximity, Aspect, and Hillshade exhibited only moderate to weak influence (V = 0.37–0.43).Overall, these results are consistent with the findings of Pande et al. (2018), who identified proximity to roads and settlements as primary drivers of agricultural and urban/village expansion.

The Cramér's V importance values for all driver variables across all temporal intervals were further analyzed. Overall, distance to settlements (mean importance = 174.14 for 3-year and 202.58 for 5-year intervals) and elevation (DEM; mean importance = 228.23 for 5-year and 179.87 for 10-year intervals) shown the strongest influential drivers of LULC change, consistent across all three temporal intervals. Distance to roads ranked among the top three drivers across all intervals (mean importance = 169.21 for 3-year, 202.82 for 5-year, and 124.65 for 10-year). For the 3-year interval, the ranking was distance to settlements followed by DEM and distance to roads respectively, reflecting the dominance of accessibility driven agricultural expansion near established communities. In contrast, during the 5-year interval, DEM ranked highest, followed by distance to roads and distance to settlements, suggesting that topographic constraints become more pronounced over longer calibration periods. Similarly, the 10-year interval, DEM remained the most influential variable, followed by distance to settlements and aspect ranging second and third, respectively, indicating the combined influence of physical terrain and accessibility in long-term transition dynamics. Collectively, these findings reinforce the assertion that proximity to human infrastructure acts as the primary catalyst for forest-to-agriculture conversion, while topographic factors modulate the spatial patterns and intensity of land-use change in mountainous landscape.

Prior to model implementation, multicollinearity among the seven driver variables was assessed using a pairwise Cramér's V matrix **(Table 7)**. The highest correlation was observed between Aspect and Hillshade (V = 0.46), followed by Slope and Hillshade (V = 0.23). All remaining pairwise association exhibited the values below 0.20, confirming that the selected drivers factors provide largely independent explanatory contributions and can therefore be retained in the transition suitability modeling framework without significant multicollinearity concerns.

Table 7.

Cramér's V Correlation Matrix Between Driver Variables.

	Aspect	DEM	Hillshade	Dist.Rd	Slope	Dist.Str	Dist.Set
Aspect	1.0000	0.0355	0.4628	0.0441	0.0571	0.0599	**0.0511**
DEM	0.0355	1.0000	0.0361	0.1382	0.0522	0.0889	**0.1570**
Hillshade	0.4628	0.0361	1.0000	0.0491	0.2348	0.0658	**0.0625**
Dist. Roads	0.0441	0.1382	0.0491	1.0000	0.0802	0.0658	**0.1492**
Slope	0.0571	0.0522	0.2348	0.0802	1.0000	0.0626	**0.0738**
Dist. Streams	0.0599	0.0889	0.0658	0.0658	0.0626	1.0000	**0.0720**
Dist. Settle.	0.0511	0.1570	0.0625	0.1492	0.0738	0.0720	**1.0000**

4.4. Transition Probability Matrix (TPM) and Model Validation

The transition probability matrix for 2006–2016 period indicates that forest exhibited a highest degree of stability, retaining 74.73% of its original area, with the largest conversion towards Grassland (9.19%) and Urban/Village (8.58%). Agriculture showed moderate persistence, with 46.49% remaining unchanged, accompanied by a substantial conversion to Urban/Village (26.25%). Grassland exhibited the highest stability (67.32%), while Degraded Forest showed strong reversion to Forest (38.83%) and Urban/Village (37.50%).

During 2016–2026 period, Forest retention dropped to 54.05%, with 24.59% converting to Agriculture, reflecting accelerated agricultural expansion. Agriculture maintained a retention rate of 58.70%. Grassland showed substantial reversion to Forest (54.89%), while Degraded Forest continued to convert primarily to Forest (38.04%) and Agriculture (40.53%).

Table 8.

Transition Probability Matrices for the three temporal intervals.

Interval	From \ To	Forest	Agriculture	Urban/Village	Grassland	Degraded
3-year (2020 to 2023)	**Forest**	**0.7425**	0.0869	0.0928	0.0543	0.0234
	Agriculture	0.0232	**0.8266**	0.0711	0.0021	0.0770
	Urban/Village	0.2705	0.2469	**0.3831**	0.0176	0.0819
	Grassland	0.4921	0.0593	0.0513	**0.3911**	0.0063
	Degraded	0.0696	0.4253	0.2566	0.0014	**0.2471**
5-year (2016 to 2021)	**Forest**	**0.6950**	0.0980	0.0877	0.0908	0.0286
	Agriculture	0.0624	**0.6286**	0.0785	0.0036	0.2269
	Urban/Village	0.2076	0.3639	**0.2675**	0.0161	0.1449
	Grassland	0.5909	0.1382	0.1201	**0.1032**	0.0476
	Degraded	0.3467	0.2910	0.1842	0.0080	**0.1700**
10-year (2006 to 2016)	**Forest**	**0.7473**	0.0228	0.0858	0.0919	0.0522
	Agriculture	0.0817	**0.4649**	0.2625	0.1165	0.0744
	Urban/Village	0.3296	0.1247	**0.4005**	0.0528	0.0924
	Grassland	0.1829	0.0368	0.0620	**0.6732**	0.0452
	Degraded	0.3883	0.0778	0.3750	0.0383	**0.1206**

Diagonal values (highlighted) represent class retention probability. Off-diagonal values represent transition probability to other classes.

Table 9.

Olofsson Unbiased Area Estimates (ha).

Class	Mapped (ha)	Unbiased (ha)	SE (ha)	CI95 Lower	CI95 Upper
Forest	15093	12257	337	11596	**12918**
Agriculture	10013	12070	431	11224	**12915**
Urban/Village	1698	1553	182	1196	**1909**
Grassland	2812	2067	141	1791	**2342**
Degraded Forest	3541	5210	364	4496	**5924**

The Olofsson unbiased area estimates for 5-year interval, validated against the 2026reference data, are presented in **Table 9** and reveal notable discrepancies between mapped and corrected land-use areas. Agricultural land was substantially underestimated by the classified map of 10,013 ha compared to an Unbiased estimated of 12,070 ha. Whereas, forest area was overestimated (mapped: 15,093 ha; unbiased: 12,257 ha). Degraded Forest showed the largest relative underestimation (mapped: 3,541 ha; unbiased: 5,210 ha). The Olofsson correction was applied to the 5-year interval as a representative example, however, the same methodological approach can be extended to other temporal intervals in future analyses.

The correspondence between the simulated land-use map for 2026 and the reference dataset derived from visual interpretation of Sentinel-2 satellite imagery for the same year was examined. Such comparison between the simulated output and empirical observations are essential for verifying the accuracy of the spatial transition probability model and for determining the applicability of the Transition Matrices for future projections under the BAU scenario across all three temporal intervals.

The two-period BAU comparison approach adopted in this study follows the framework proposed by Hamad et al. (2018) and provides critical insights into the temporal stationarity assumption underlying Markov-based models. The pronounce performance difference, observed for the 10-year intervals, between BAU-Early (FOM = 0.153) and BAU-Recent (FOM = 0.318) demonstrates that transition probabilities are non-stationary over extended time horizons. This finding carried important methodological implications for CA–Markov applications. Consistent with this result, Aburas et al. (2019) identified the assumption of temporal stationarity is the primary limitation of Markov-based models, particularly when calibration periods encompass the phases of rapid socio-economic change.

The projected continued decline in forest cover under all BAU scenarios carries significant implications for ecosystem service provision within the Salween and Ping watershed system. According to Wang et al. (2023), the conversion of high-integrity forests to cropland is accelerating globally, with tropical highland regions identified as particularly vulnerable. In Thailand, the Royal Project system was established precisely to encounter this trajectory by promoting sustainable highland agriculture as an alternative to shifting cultivation. However, the discrepancy between the Royal Project's conservation mandate and the continued deforestation observed in this study suggests that existing interventions may be insufficient to offset persistent market-driven pressures for agricultural expansion.

Future land-use development would benefit from moving beyond the BAU assumption by incorporating policy intervention scenarios simulation. Gebresellase et al. (2023) demonstrated that integrating alternative policy intervention into CA–Markov framework produces more realistic and decision-relevant predictions than single-scenario approaches. Such an extension would allow stakeholders to evaluate the potential effectiveness of measures cush as buffer zones, agroforestry programs, and conservation agriculture initiatives in mitigating the projected deforestation trajectory.

The validation of the 2026 land-use projection indicated that the 3-year interval model achieved the highest accuracy (OA = 0.6592, Kappa = 0.4922, FOM = 0.3254), followed by the 5-year model (OA = 0.6160, Kappa = 0.4134, FOM = 0.3432) and the 10-year model (OA = 0.3940, Kappa = 0.1141, FOM = 0.1527). At this class level, notable discrepancies were observed for the forest and agriculture categories, where the simulations projected greater forest loss and agricultural expansion than were evident in the data. This deviation likely reflects model assumptions that assigned relatively high important to accessibility of drivers and agricultural suitability. Nevertheless, the proportions for Urban/Village, Grassland, and Degraded Land closely remained with observed values, demonstrating the model's capacity to forecast overall trends, as shown in **Table 10.**

Table 10.

CA-Markov Model Validation Metrics - 2026 Reference.

Metric	3-Year	5-Year	10-Year
Overall Accuracy (OA)	0.6592	0.6160	0.3940
Kappa Coefficient	0.4922	0.4134	0.1141
Figure of Merit (FOM)	0.3254	0.3432	0.1527
Quantity Disagreement	0.1060	0.1556	0.2852
Allocation Disagreement	0.2348	0.2284	0.3208
Hit (A)	343	406	246
Miss (B)	538	596	1264
False Alarm (C)	173	181	101

The moderate Kappa values obtained in this study (0.49 for the 3-year and 0.41 for the 5-year interval) require contextualization within the broader CA–Markov modeling literature. Although these values are lower than those reported in some studies, for instance, Aburas et al. (2019) achieved Kappa as 0.80 for urban expansion prediction in Egypt using only four LULC classes, they remain comparable to results reported for complex mountainous landscapes. Gasirabo et al. (2023) reported a Figure of Merit of 0.19 for a 6-class CA–Markov model applied to the Nyabarongo River Basin in Rwanda, and similarly concluded that model performance deteriorates with increasing landscape heterogeneity and classification complexity. Several factors specific to this study likely contributed to moderate accuracy. First, the use of five LULC classes compared to three or four commonly employed in many previous studies, increases the potential for spectral confusion, particularly between Urban/Village and Degraded Forest, which exhibit similar spectral characteristic in both Landsat and Sentinel-2 imagery (Aftab et al., 2024). Second, the complex terrain of the Loe Tor area (elevations 219–1,464 m) introduces topographic shadowing and aspect-dependent reflectance variations that amplify classification uncertainty (Shandu et al., 2025). Third, the multi-sensor integration between Landsat (30 m) and Sentinel-2 (10 m resampled to 30 m) introduces spectral response inconsistencies that propagate into transition probability matrices (Claverie et al., 2018).

Nevertheless, the 3-year model's FOM (0.33) exceeds the benchmark range of 0.05–0.30 typically reported for CA–Markov simulations (Pontius et al., 2007), confirming the model ability to captures the dominant forest-to-agriculture conversion trajectory. Consistent with these finding, Kundu and Kumar (2024) similarly demonstrated that predictive accuracy generally declines as the calibration interval length increase, consistent with this finding that the 10-year model (Kappa = 0.11) performed substantially worse than the 3-year model. Detailed confusion matrices for all three intervals are provided in **(Table 11).**

Table 11.

Confusion Matrix 3-Year, 5-Year, 10-Year Interval.

Confusion Matrix 3-Year Interval.

Predicted \ Reference	Forest	Agriculture	Urban/Village	Grassland	Degraded
Forest	913	103	32	109	36
Agriculture	69	569	36	14	116
Urban/Village	93	85	43	12	62
Grassland	35	3	0	77	1
Degraded	9	34	3	0	46

Confusion Matrix 5-Year Interval.

Predicted \ Reference	Forest	Agriculture	Urban/Village	Grassland	Degraded
Forest	934	187	50	144	80
Agriculture	62	461	34	16	60
Urban/Village	74	90	27	7	37
Grassland	12	5	0	48	0
Degraded	44	54	4	0	70

Confusion Matrix 10-Year Interval.

Predicted \ Reference	Forest	Agriculture	Urban	Grassland	Degraded
Forest	769	385	81	141	90
Agriculture	18	113	10	0	70
Urban/Village	123	150	30	10	80
Grassland	191	64	5	59	13
Degraded	37	43	2	2	14

4.5. Future LULC Projections and BAU Scenarios

Future projections indicate that Forest cover is predicted to decline from 12,113.40 ha (2026*), to 10,363.15 ha by 2036*, followed by a partially recovery to 11,699.61 ha by 2056*. Agricultural land expands markedly from 1,606.61 ha (2026*) to a peak of 4,070.01 ha (2036*), before moderating to 2,347.84 ha by 2056*. In contrast, Urban/Village, Grassland, and Degraded Forest classes exhibit relatively stable extents, with only minor inflection throughout the projection period. It is important to noted that the apparent Forest cover recovery in the 10-year BAU-Early projections (2046–2056) represents an artifact rather than a genuine ecological trend. This arises from sensor inconsistency within the 10-year interval calibration interval, which incorporates data from Landsat 5 TM (2006), Landsat 8 OLI (2016), and Sentinel-2 MSI (2026), three sensors with different spectral responses and spatial resolutions. For example, Urban/Village area fluctuated from 2,010 ha (2006, Landsat 5) to 3,240 ha (2016, Landsat 8) before declining sharply to 990 ha (2026, Sentinel-2), a pattern inconsistent with field observations and attributable to sensor-dependent classification differences. Consequently, The T1 to T2 Markov transition matrix recorded an anomalously high Urban-to-Forest transition probability (0.330), which generated the spurious forest recovery signal in long-term projections. In contrast, the BAU-recent scenario (T2 to T3), which relies solely on the Landsat 8 to Sentinel-2 transition, provides greater internal consistency and is recommended as the primary projection scenario for the 10-year interval.

The transition sample analysis confirmed that sufficient training samples were available for all 20 transition pairs, with sample sizes ranging from 101 (Grassland to Agriculture) to 2,316 (Forest to Grassland). Predicted LULC areas under the 10-year BAU-Early scenario are summarized in (**Table 12**). All transitions with Markov probability exceeding 0.02 were successfully modeled.

Table 12.

Predicted LULC areas (ha) for 2026 (predicted), 2036, 2046, and 2056.

LULC Class	2026* (ha)	2036* (ha)	2046* (ha)	2056* (ha)
Forest	12113.40	10363.15	11189.17	**11699.61**
Agriculture	1606.61	4070.01	2952.30	**2347.84**
Urban/Village	3001.23	2460.85	2801.17	**2814.46**
Grassland	2676.80	2231.48	2534.91	**2733.94**
Degraded Forest	759.58	1032.13	680.07	**561.77**

* *Predicted values.*

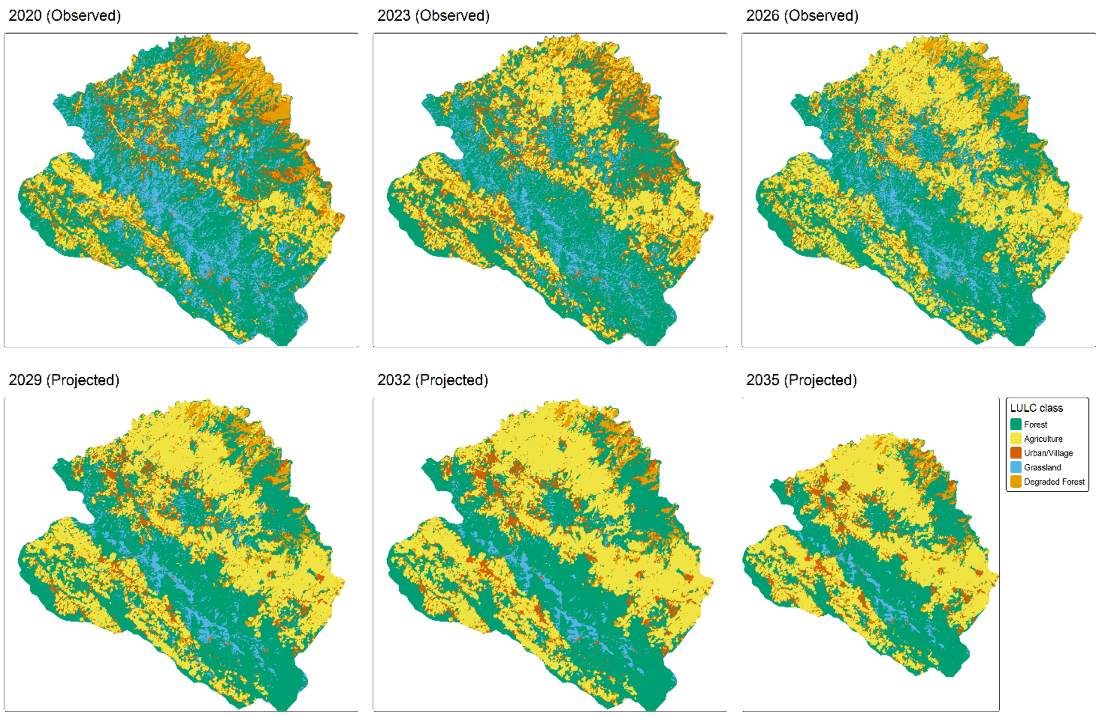

Fig. 4. Observed (2020, 2023, 2026) and 3-year BAU-Recent projected (2029, 2032, 2035) LULC maps, Loe Tor Royal Project.

Under the 10-year BAU scenario, the Forest cover is projected to decline from 12,921.8 ha (64.10%) in 2006 to 10,363.15 ha by 2036, followed by a partial recovery to 11,699.61 ha by 2056. In contrast, the 3-year BAU scenario exhibits a more severe and consistently declining trajectory, with Forest reduce from 9,867.4 ha (2020) to 8,356 ha by 2035. It is important to noted that the apparent forest recovery observed in the 10-year BAU-Early scenario does not reflect plausible ecological dynamics. As discussed in Section 3.4, this recovery arises from artifacts introduced by multi-sensor transition probability estimation and should therefore be interpreted with caution.

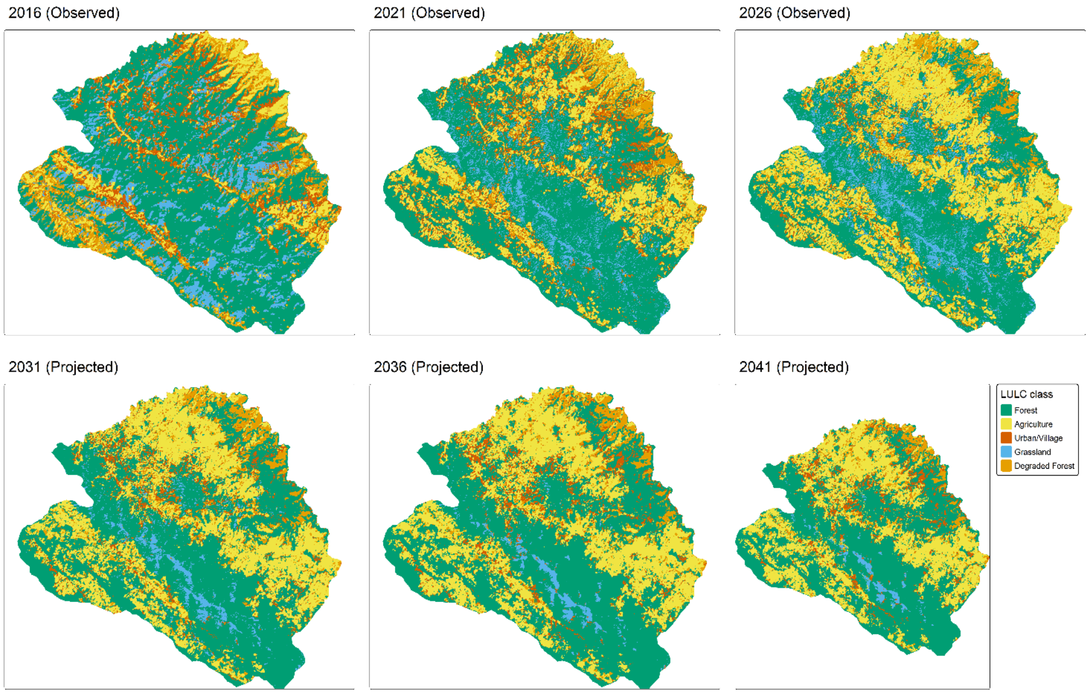

Fig. 5. Observed (2016, 2021, 2026) and 5-year BAU-Recent projected (2031, 2036, 2041) LULC maps.

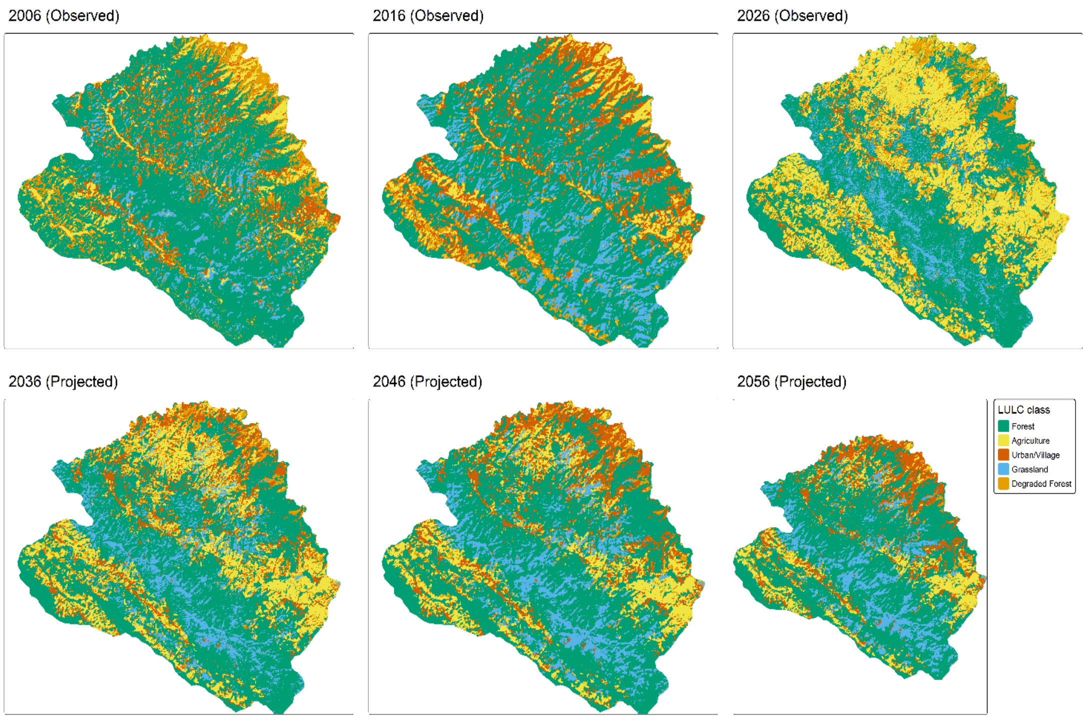

Fig. 6. Observed (2006, 2016, 2026) and 10-year BAU-Recent projected (2036, 2046, 2056) LULC maps; BAU-Recent is shown to avoid the cross-sensor artifact (see Section 3.5).

The 10-year BAU-Recent scenario, which relies exclusively on the Landsat 8 to Sentinel-2 transition matrix, provides a more ecologically realistic projection and indicates a continued decline in forest cover consistent with trends observed in the 3-year and 5-year interval. Projected LULC maps under the 3-year, 5-year, and 10-year BAU-Recent scenarios are illustrated in (**Figs. 3, 4, and 5**), respectively. Overall, this scenario reflects a cumulative forest loss across 4,400 hectares, equivalent to around 22% of the original forest area, highlights a high degree of ecosystem vulnerability and may directly impact on the ecological balance, specifically regarding biodiversity, carbon sequestration, and the maintenance of the hydrological cycle.

In contrast, the agricultural land expanded continuously from 1,671.0 ha (8.29%) in 2006 to 6,213.0 ha (30.82%) in 2026 under the 10-year interval, representing a net gain of 4,542.0 ha (+227.1 ha/yr). The expansion rate was more pronounced during the most recent 3-year interval (2020–2026) reaching +518.4 ha/yr, indicating an accelerating conversion of forested land to agriculture. This rapid expansion is largely driven by economic incentives and raising demand for agricultural production, particularly in foothill regions characterized by favorable topography and road infrastructure. Consequently, forest-to-agriculture conversion emerged as the primary mechanism driving LULC dynamics in the region.

On the contrary, Urban/Village areas exhibited a high degree of spatial stability, remaining relatively constant at approximately 990 ha (4.91% in 2026). This stability indicates that the urban expansion is not a primary driver of recent Land Use and Land Cover (LULC) change in this specific region. Similarly, Degraded forest maintained relatively stable trends across the BAU projections, accounting for approximately 10.42% of the study area in 2026. Nevertheless, under the 10-year scenario, Degraded Forest is projected to decline from 1,032 ha in 2036 to 562 ha by 2056, indicating a gradual transition toward other land-cover types.

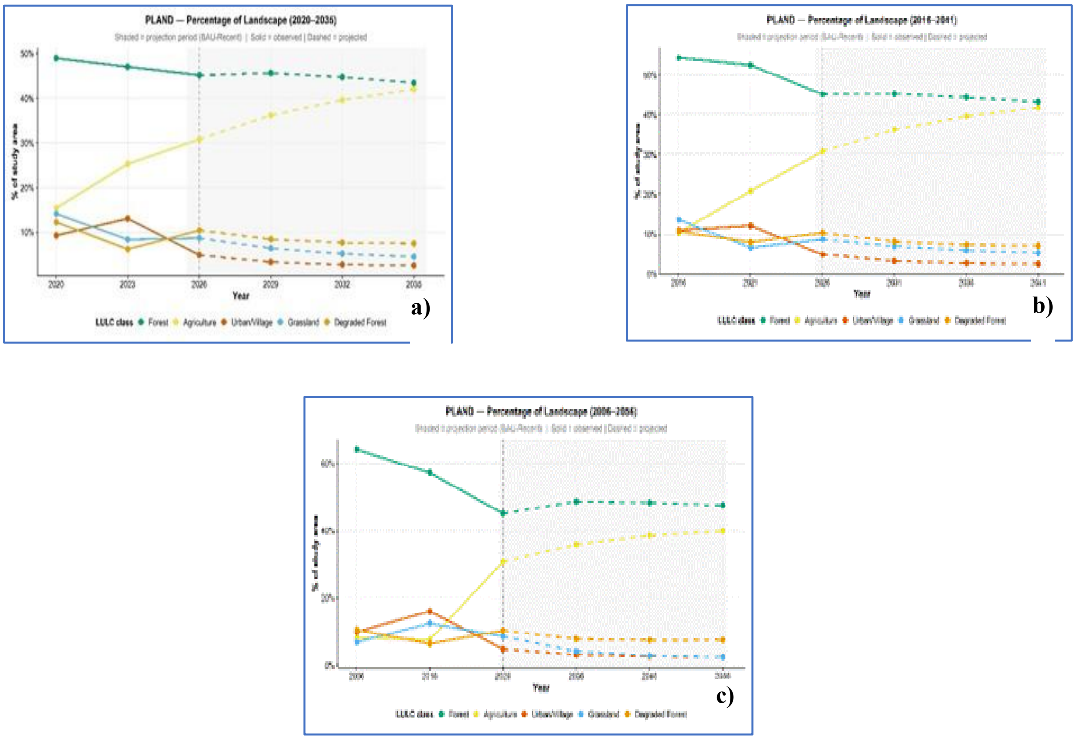

Fig. 7. Percentage-of-landscape (PLAND) trends for the five LULC classes under BAU-Recent: (a) 3-year, (b) 5-year, (c) 10-year interval. The vertical dashed line marks the observed-to-projected boundary (2026).

Grassland demonstrated instability across all BAU projections. Under the 3-year scenario, Grassland is projected to decline sharply from 1,750.7 ha in 2026 to 483 ha by 2035. In contrast, the 10-year projection indicate more moderate fluctuations ranging between 2,231 and 2,734 ha through 2056. These contrast behavior likely reflect the uncertainty of land-use dynamics at the transitional interface between agriculture and forestry. PLAND trends for all LULC classes across all BAU-Recent scenarios are shown in (**Fig. 7**).

Following Hamad et al. (2018), two Business As Usual (BAU) scenarios were defined for each temporal interval: BAU-Early, which applies the transition probability matrix derived from the T1 to T2 period, and BAU-Recent, which applies the matrix derived from the T2 to T3 period. For the 3-year interval, BAU-Early (P_2020 to 2023) yielded FOM of 0.325, whereas BAU-Recent (P_2023 to 2026) produced FOM of 0.312. Both scenarios performed similarly, with BAU-Early exhibiting a marginally higher FOM but comparable OA and Kappa values.

For the 5-year interval, BAU-Early (P_2016 to 2021) yielded an OA of 0.614, Kappa of 0.396, and FOM of 0.286, whereas BAU-Recent (P_2021 to 2026) achieved OA of 0.627, Kappa of 0.432, and FOM of 0.299. The BAU-Recent scenario consistently outperformed BAU-Early across all key metrics and presented substantially lower Quantity Disagreement (0.056 vs. 0.146).

For the 10-year interval, BAU-Early (P_2006 to 2016) yielded a FOM of 0.153, whereas BAU-Recent (P_2016 to 2026) produced a substantially higher FOM of 0.318. This large discrepancy reflects the previous discussed multi-sensor artifact, whereby BAU-Early contains an anomalous high Urban-to-Forest transition probability (0.330) resulting from cross-sensor Landsat 5 to Landsat 8 classification differences, leading to spurious Forest recovery in long-term projections. In contrast, BAU-Recent, based solely on the Landsat 8–to–Sentinel-2 matrix, avoids this artifact and is therefore recommended as the primary scenario. A visual comparison of BAU-Early and BAU-Recent projections across all intervals is presented in (**Fig. 8**).

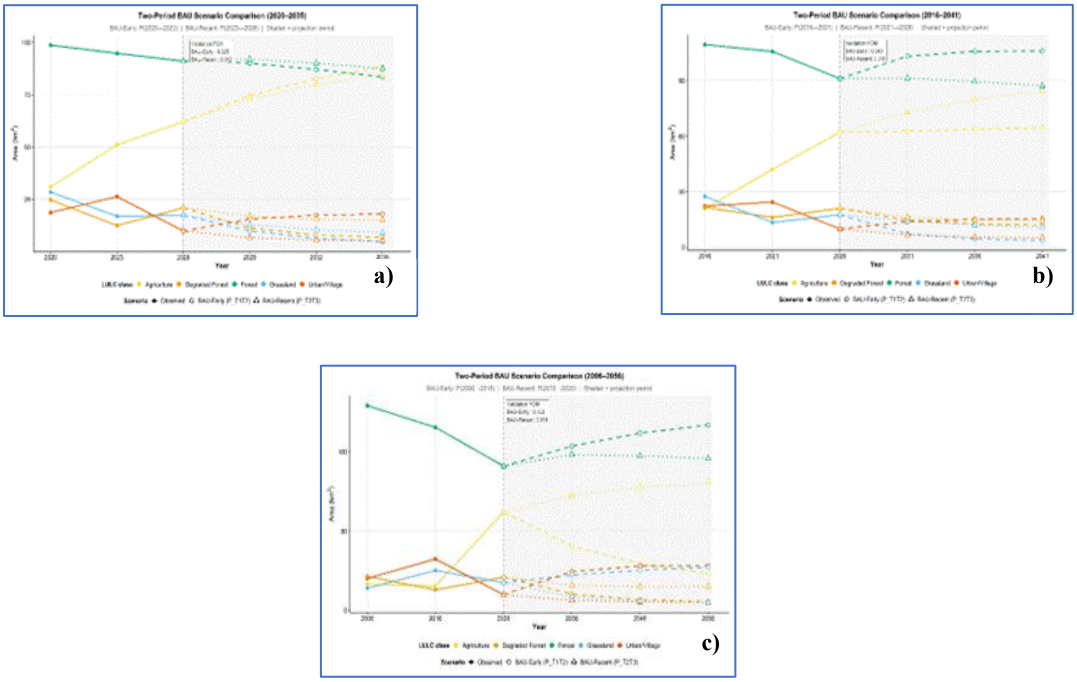

Fig. 8. Two-period BAU comparison — BAU-Early (P_T1→T2) versus BAU-Recent (P_T2→T3) — across the (a) 3-year, (b) 5-year, and (c) 10-year intervals.

In terms of class-specific accuracy, Forest consistently achieved the highest F1 scores across all intervals (F1 = 0.59–0.79), followed by Agriculture (F1 = 0.23–0.71). Urban/Village and Degraded Forest classes exhibited substantial confusion with other classes, resulting in lower F1 scores (F1 = 0.08–0.26 for Degraded Forest; F1 = 0.12–0.21 for Urban/Village). This reflects the model's limitations in distinguishing between land-uses classes with similar spectral characteristics or subtle spatial differences. However, in terms of overall precision, the model is considered sufficiently reliable for forecasting future land-use changes.

The validation analysis further indicates that while the model successfully captures a substantial number of predicted areas (Hits) across classes, False Alarms and Misses were also prevalent. These errors were particularly evident in the transitions of Forest-to-Agriculture and Forest-to-Degraded Land, which represent the dominant change process in the study area. False Alarms suggests an overestimation in certain classes, while Misses reflect underestimation of actual changes. Nevertheless, the spatial distribution of Hits indicates that the model adequately captures overall LULC trends.

4.6. Landscape Fragmentation Analysis

Landscape-level metrics were computed using the landscape metrics package in R for all observed years (2006, 2016, 2021, 2026) and projected years under the BAU-Recent scenario (5-year interval: 2031, 2036, 2041). Three complementary indices were evaluated: Shannon's Diversity Index (SHDI), Contagion Index (CONTAG), and Patch Density (PD). The results indicate a consistent decline in landscape diversity over the observed period. SHDI decreased from 1.417 (2006) to 1.294 (2016) and 1.326 (2026), reflecting the progressive landscape simplification as Agriculture replaced more diverse natural cover types. Concurrently, CONTAG increased from 38.3 (2006) to 43.8 (2016), indicating increasingly aggregation of dominant agricultural class and the expansion of large contiguous farmland.

Patch Density declined from 230.0 to 179.1 patches per 100 ha over the same period, suggesting fewer but larger and more spatially concentrated patches. Under BAU-Recent projections, SHDI is expected to continue declining while CONTAG increases, consistent with ongoing agricultural consolidation at the expense of forest patch diversity. At the class level, Forest exhibited a marked increase in the Number of Patches (NP) between 2016 and 2026 (from approximately 2,972 to 4,059 patches), indicating an active fragmentation of the forest matrix into smaller and more isolated units. A corresponding decline in the Aggregation Index (AI) confirmed reduced spatial connectivity among remaining forest patches, with implications for biodiversity persistence and ecosystem functioning.

The observed increase in forest patch number (from 2,972 to 4,059 patches between 2016 and 2026) coupled with declining Aggregation Index, represents a classic fragmentation trajectory widely documented in tropical montane forests. Chidodo et al. (2025) reported similar patterns in the East Usambara Mountains of Tanzania, where agricultural encroachment progressively fragmented contiguous forest blocks into smaller and more isolated patches. The ecological consequences of such fragmentation are well-established: reduced patch size limited habitat availability for area-sensitive species, while increased edge-to-interior ratio alters microclimate conditions and facilitate invasion by pioneer species (Haddad et al., 2015).

The declining in Shannon Diversity Index (SHDI from 1.417 to 1.326) indicates progressive landscape simplification, consistent with the dominance of forest-to-agriculture conversion as a single prevailing transition pathway. This pattern contrasts with landscapes experiencing multiple simultaneous transitions (e.g., urbanization combined with agricultural expansion), which typically exhibit stable or increasing SHDI values (Gasirabo et al., 2023). The concurrent increase in CONTAG (from 38.3 to 43.8) further confirms that agricultural expansion is creating large, contiguous farmland blocks rather than dispersed patches, a pattern with potentially irreversible implications for forest connectivity and wildlife corridor viability in the Salween and Ping watersheds.

5. CONCLUSIONS

This study integrated multi-temporal satellite imagery, five supervised classification algorithms, and CA‑Markov modelling to analyse LULC dynamics in the Loe Tor Royal Project area between 2006 and 2026. The results reveal a consistent and accelerating loss of forest to agriculture, with proximity to settlements and roads identified as the primary spatial drivers. Sentinel-2 consistently outperformed Landsat, and no single classifier was superior across all years, underscoring the sensitivity of classifier performance to sensor characteristics and landscape complexity.

The comparison of calibration intervals is the principal methodological contribution. The 3-year interval produced the most reliable CA‑Markov projections, substantially outperforming the 5- and 10-year models; the poor performance of the 10-year model is attributable to Markov non-stationarity and cross-sensor spectral inconsistency over long horizons. Across all Business-as-Usual scenarios, forest cover is projected to continue declining while agriculture expands along low-elevation margins near roads and settlements.

These findings should be read against three limitations: cross-sensor integration introduces spectral-response differences that affect transition estimation (notably for the 10-year interval); minor classes (Urban/Village, Degraded Forest) remain affected by spectral confusion in complex terrain; and the BAU projections assume stationary transition rates without explicit policy or climate drivers. Within these bounds, the study points to three priority interventions − protective buffer zones around remaining forest, conservation agriculture as an alternative to forest conversion, and GIS-based monitoring for proactive management − and provides methodological guidance for CA‑Markov applications in tropical mountainous landscapes. Future work should incorporate socio-economic drivers and compare CA‑Markov with alternative modelling frameworks.

6. DATA AVAILABILITY

The Landsat imagery is freely available from the USGS Earth Explorer (https://earthexplorer.usgs.gov). Sentinel-2 Level-2A imagery was obtained from the Copernicus Open Access Hub (https://dataspace.copernicus.eu). The R scripts used for classification and CA–Markov modeling is available from the corresponding author upon reasonable request.

ACKNOWLEDGEMENTS

This study was conducted under the auspices of the Princess Sirindhorn Center for Sustainable Development, Kasetsart University. The authors also gratefully acknowledge the Royal Project Foundation and the Land Development Department (LDD) for providing field reference data and local land-use information. Satellite imagery was obtained free of charge from the Copernicus Open Access Hub (European Space Agency) and the United States Geological Survey (USGS) Earth Explorer. This research received no specific grant from any funding agency in the public, commercial, or nonprofit sectors.

REFERENCES

Aburas, M. M., Ahamad, M. S. S. and Omar, N. Q. (2019). "Spatio-temporal simulation and prediction of land-use change using conventional and machine learning models: a review." *Environ Monit Assess* **191**(4): 205. Available from: https://doi.org/10.1007/s10661-019-7330-6 [Accessed 5 March 2026].

Aftab, B., Wang, Z., Wang, S. and Feng, Z. (2024). "Application of a Multi-Layer Perceptron and Markov Chain Analysis-Based Hybrid Approach for Predicting and Monitoring LULCC Patterns Using Random Forest Classification in Jhelum District, Punjab, Pakistan." *Sensors (Basel)* **24**(17): 5648. Available from: https://doi.org/10.3390/s24175648 [Accessed 30 August 2025].

Akoglu, H. (2018). "User's guide to correlation coefficients." *Turk J Emerg Med* **18**(3): 91-93. Available from: https://doi.org/10.1016/j.tjem.2018.08.001 [Accessed 1 September 2025].

Bai, M., Zhang, X., Ai, W., Jing, X. and Liu, L. (2025). "A high-resolution global annual city and town boundaries dataset (2000-2022) derived from GLC_FCS30D product." *Sci Data* **13**(1): 50. Available from: https://doi.org/10.1038/s41597-025-06368-9 [Accessed 4 December 2025].

Bairwa, B., Sharma, R., Kundu, A., Sammen, S. S., Alshehri, F., Pande, C. B., Orban, Z. and Salem, A. (2025). "Predicting changes in land use and land cover using remote sensing and land change modeler." *Frontiers in Environmental Science* **13**: 1540140. Available from: https://doi.org/10.3389/fenvs.2025.1540140 [Accessed 1 March 2026].

Basheer, S., Wang, X., Farooque, A. A., Nawaz, R. A., Liu, K., Adekanmbi, T. and Liu, S. (2022). "Comparison of Land Use Land Cover Classifiers Using Different Satellite Imagery and Machine Learning Techniques." *Remote Sensing* **14**(19): 4978. Available from: https://doi.org/10.3390/rs14194978 [Accessed 1 March 2026].

Butt, A., Shabbir, R., Ahmad, S. S. and Aziz, N. (2015). "Land use change mapping and analysis using Remote Sensing and GIS: A case study of Simly watershed, Islamabad, Pakistan." *The Egyptian Journal of Remote Sensing and Space Science* **18**(2): 251-259. Available from: https://doi.org/10.1016/j.ejrs.2015.07.003 [Accessed 30 December 2025].

Chidodo, S., Zhang, L., Zarei, A. and Feger, K.-H. (2025). "Remote sensing-based assessment of four decades of land use/land cover change in the Sigi River Watershed, East Usambara Mountains, Tanzania." *Frontiers in Remote Sensing* **6**: 1594331. Available from: https://doi.org/10.3389/frsen.2025.1594331 [Accessed 30 January 2026].

Claverie, M., Ju, J., Masek, J. G., Dungan, J. L., Vermote, E. F., Roger, J.-C., Skakun, S. V. and Justice, C. (2018). "The Harmonized Landsat and Sentinel-2 surface reflectance data set." *Remote Sensing of Environment* **219**: 145-161. Available from: https://doi.org/10.1016/j.rse.2018.09.002 [Accessed 1 March 2026].

Cochran, W. G. (1950). "The comparison of percentages in matched samples." *Biometrika* **37**(3-4): 256-266. Available from: https://doi.org/10.1093/biomet/37.3-4.256 [Accessed 20 April 2026].

Cohen, J. (1960). "A Coefficient of Agreement for Nominal Scales." *Educational and Psychological Measurement* **20**(1): 37-46. Available from: https://doi.org/10.1177/001316446002000104 [Accessed 1 March 2026].

Congalton, R. G. (2001). "Accuracy assessment and validation of remotely sensed and other spatial information." *International Journal of Wildland Fire* **10**(4): 321-328. Available from: https://doi.org/10.1071/wf01031 [Accessed 1 March 2025].

Gasirabo, A., Xi, C., Hamad, B. R. and Edovia, U. D. (2023). "A CA–Markov-Based Simulation and Prediction of LULC Changes over the Nyabarongo River Basin, Rwanda." *Land* **12**(9): 1788. Available from: https://doi.org/10.3390/land12091788 [Accessed 30 March 2026].

Gebresellase, S. H., Wu, Z., Xu, H. and Muhammad, W. I. (2023). "Scenario-Based LULC Dynamics Projection Using the CA–Markov Model on Upper Awash Basin (UAB), Ethiopia." *Sustainability* **15**(2): 1683. Available from: https://doi.org/10.3390/su15021683 [Accessed 30 March 2026].

Haddad, N. M., Brudvig, L. A., Clobert, J., Davies, K. F., Gonzalez, A., Holt, R. D., Lovejoy, T. E., Sexton, J. O., Austin, M. P., Collins, C. D., Cook, W. M., Damschen, E. I., Ewers, R. M., Foster, B. L., Jenkins, C. N., King, A. J., Laurance, W. F., Levey, D. J., Margules, C. R., Melbourne, B. A., Nicholls, A. O., Orrock, J. L., Song, D.-X. and Townshend, J. R. (2015). "Habitat fragmentation and its lasting impact on Earths ecosystems." *Science Advances* **1**(2): e1500052. Available from: https://doi.org/10.1126/sciadv.1500052 [Accessed 30 March 2026].

Hamad, R., Balzter, H. and Kolo, K. (2018). "Predicting Land Use/Land Cover Changes Using a CA-Markov Model under Two Different Scenarios." *Sustainability* **10**(10): 3421. Available from: https://doi.org/10.3390/su10103421 [Accessed 30 March 2026].

Hurni, K. and Fox, J. (2018). "The expansion of tree-based boom crops in mainland Southeast Asia: 2001 to 2014." *Journal of Land Use Science* **13**(1-2): 198-219. Available from: https://doi.org/10.1080/1747423x.2018.1499830 [Accessed 30 March 2026].

Keyamf, C., Yemefack, M., Silatsa, F. and Oben, T. (2023). "Sentinel-2 and Landsat-8 potentials for high-resolution mapping of the shifting agricultural landscape mosaic systems of Southern Cameroon." *International Journal of Applied Earth Observation and Geoinformation* **124**: 103545. Available from: https://doi.org/10.1016/j.jag.2023.103545 [Accessed 1 November 2025].

Kiriwongwattana, K. and Waiyasusri, K. (2024). "Spatial evolution of smart cities for sustainable tourism: A case study of phuket province, thailand." *GeoJournal of Tourism and Geosites* **55**: 1312-1320. Available from: https://doi.org/10.30892/gtg.55331-1303 [Accessed 30 June 2026].

Kundu, S. and Kumar, V. (2024). "Significance of Measuring the Accuracy of Cellular Automata Markov Chain for Land Use Projections in District Gurgaon in Haryana, India." *International Journal of Engineering Trends and Technology* **72**(9): 304-311. Available from: https://doi.org/10.14445/22315381/ijett-v72i9p125 [Accessed 30 April 2026].

Madiela, B., Clobite, B. and Midel, M. (2024). "Comparing Sentinel-2 and Landsat 9 for land use and land cover mapping assessment in the north of Congo Republic: a case study in Sangha region." *International Journal of Remote Sensing* **45**: 1-22. Available from: https://doi.org/10.1080/01431161.2024.2394238 [Accessed 1 October 2025].

Mansour, S., Al-Belushi, M. and Al-Awadhi, T. (2020). "Monitoring land use and land cover changes in the mountainous cities of Oman using GIS and CA-Markov modelling techniques." *Land Use Policy* **91**: 104414. Available from: https://doi.org/10.1016/j.landusepol.2019.104414 [Accessed 1 August 2025].

Mohanrajan, S. N., Loganathan, A. and Manoharan, P. (2020). "Survey on Land Use/Land Cover (LU/LC) change analysis in remote sensing and GIS environment: Techniques and Challenges." *Environ Sci Pollut Res Int* **27**(24): 29900-29926. Available from: https://doi.org/10.1007/s11356-020-09091-7 [Accessed 15 August 2025].

Nouri, J., Gharagozlou, A., Arjmandi, R., Faryadi, S. and Adl, M. (2014). "Predicting Urban Land Use Changes Using a CA–Markov Model." *Arabian Journal for Science and Engineering* **39**(7): 5565-5573. Available from: https://doi.org/10.1007/s13369-014-1119-2 [Accessed 30 November 2025].

Olofsson, P., Foody, G. M., Herold, M., Stehman, S. V., Woodcock, C. E. and Wulder, M. A. (2014). "Good practices for estimating area and assessing accuracy of land change." *Remote Sensing of Environment* **148**: 42-57. Available from: https://doi.org/10.1016/j.rse.2014.02.015 [Accessed 25 November 2025].

Pande, C. B., Moharir, K. N., Khadri, S. F. R. and Patil, S. (2018). "Study of land use classification in an arid region using multispectral satellite images." *Applied Water Science* **8**(5): 164. Available from: https://doi.org/10.1007/s13201-018-0764-0 [Accessed 1 April 2026].

Pontius, R. G., Thontteh, O. and Chen, H. (2007). "Components of information for multiple resolution comparison between maps that share a real variable." *Environmental and Ecological Statistics* **15**(2): 111-142. Available from: https://doi.org/10.1007/s10651-007-0043-y [Accessed 30 March 2026].

Pontius, R. G. J. and Millones, M. (2011). "Death to Kappa: birth of quantity disagreement and allocation disagreement for accuracy assessment." *International Journal of Remote Sensing* **32**(15): 4407-4429. Available from: https://doi.org/10.1080/01431161.2011.552923 [Accessed 30 March 2026].

Royal Development Projects Board. 2025. *Sufficiency Economy Philosophy* [Online]. Available: https://www.rdpb.go.th/th/Sufficiency [Accessed 5 October 2025].

Royal Project Foundation. 2025. *History of Lertor Royal Project* [Online]. Available: https://royalproject.org/page/History_Lertor/ [Accessed 5 October 2025].

Sari, D. N., Mutashim, M. H. F., Restuvica, F. V., Putra, K. P. B., Mukasyaf, A. A., Anggani, N. L. and Nugraga, A. R. (2025). "Prediction of Spatial Land Use Land Cover Changes in Boven Digoel, South Papua in 2031 and 2041 Using LCM and CA-Markov Models." *Geographia Technica* **20**(2): 283-302. Available from: https://doi.org/10.21163/GT_2025.202.18 [Accessed 30 June 2026].

Shandu, I. D., Xulu, S. and Gebreslasie, M. (2025). "Enhancing land cover classification in the heterogeneous landscape by integrating auxiliary data with Sentinel-2 imagery using the random forest algorithm." *Frontiers in Remote Sensing* **6**: 1697897. Available from: https://doi.org/10.3389/frsen.2025.1697897 [Accessed 5 October 2025].

Sharma, G. and Sharma, M. K. (2024). "Development of multispectral post-classification change detection technique." *2024 IEEE International Students' Conference on Electrical, Electronics and Computer Science (SCEECS)*: 1-9. Available from: https://doi.org/10.1109/SCEECS61402.2024.10482012.

Thammanu, S., Marod, D., Han, H., Bhusal, N., Asanok, L., Ketdee, P., Gaewsingha, N., Lee, S. and Chung, J. (2020). "The influence of environmental factors on species composition and distribution in a community forest in Northern Thailand." *Journal of Forestry Research* **32**(2): 649-662. Available from: https://doi.org/10.1007/s11676-020-01239-y [Accessed 15 August 2025].

Waiyasusri, K. (2021). "Monitoring the Land Cover Changes in Mangrove Areas and Urbanization using Normalized Difference Vegetation Index and Normalized Difference Built-up Index in Krabi Estuary Wetland, Krabi Province, Thailand." *Applied Environmental Research* **43**(3): 1-16. Available from: https://doi.org/10.35762/AER.2021.43.3.1 [Accessed 30 June 2026].

Waiyasusri, K. and Chotpantarat, S. (2022). "Spatial Evolution of Coastal Tourist City Using the Dyna-CLUE Model in Koh Chang of Thailand during 1990-2050." *ISPRS International Journal of Geo-Information* **11**(1): 49. Available from: https://doi.org/10.3390/ijgi11010049 [Accessed 30 June 2026].

Wang, L., Wei, F. and Svenning, J.-C. (2023). "Accelerated cropland expansion into high integrity forests and protected areas globally in the 21st century." *iScience* **26**(4): 106450. Available from: https://doi.org/10.1016/j.isci.2023.106450 [Accessed 15 March 2026].

Worachairungreung, M., Thanakunwutthirot, K. and Kulpanich, N. (2023). "A study on oil palm classification for ranong province using data fusion and machine learning algorithms." *Geographia Technica* **18**(1): 161-176. Available from: https://doi.org/10.21163/GT_2023.181.12 [Accessed 30 June 2026].

Zhai, J., Xiao, C., Feng, Z. and Liu, Y. (2023). "Are there suitable global datasets for monitoring of land use and land cover in the tropics? Evidences from mainland Southeast Asia." *Global and Planetary Change* **229**: 104233. Available from: https://doi.org/10.1016/j.gloplacha.2023.104233 [Accessed 8 September 2025].